blurring, measured from a nearby star immediately before the start of the Pluto observations, was 0.30 arc seconds.

5. Spectra of Pluto and Charon were obtained on 28 May 1999 from 10:35 until 11:37 UT. The objects were acquired in direct imaging mode, and then, with the telescope tracking at the predicted Pluto rate on the sky, the image rotator was positioned so that Pluto and Charon fell into the 0.37–arc second–wide slit. Data acquisition and analysis were performed in a manner described in detail by M. E. Brown (*Astron. J.*, in press). Two spectral settings were required to cover the full spectral range. We acquired a total of 300 s of exposure in the HK band (1.5 to 2.5 μm) and 100 s of exposure in the JH band (1.0 to 1.6 μm). Even in the exceptionally good seeing present at the time of the observations, some light from Pluto is contained in the raw spectrum of Charon (Fig. 1). To eliminate this contribution, we subtracted the spectrum of Pluto from an equidistant point on the non-Charon side from the spectrum of Charon. This correction was equal to ~10% of the measured light from Charon. To provide a correction for atmospheric extinction, we measured the spectrum of the nearby F8V star SAO 181258 and ratioed the flux to that expected from a blackbody of equivalent temperature. This calibration star should have spectral features almost identical to those from the sun at these wavelengths [A. Lancon and B. Rocca-Volmerange, *Astron. Astrophys. Suppl. Ser.* **96**, 593 (1992)]; any spurious spectral features caused by the use of this calibrator will be smaller than a few percent of the total signal and will not be visible in the data. The spectra were scaled to absolute albedo from the data of T. L. Roush, D. P. Cruikshank, J. B. Pollack, E. F. Young, and M. J. Bartholomew [*Icarus* **119**, 214 (1996)].
6. See review by D. P. Cruikshank *et al.*, in *Pluto and Charon*, S. A. Stern and D. J. Tholen, Eds. (Univ. of Arizona Press, Tucson, AZ, 1997), pp. 221–267.
7. U. Fink and G. T. Sill, in *Comets*, L. Wilkening, Ed. (Univ. of Arizona Press, Tucson, AZ, 1982), pp. 172–202.
8. Simple extrapolation from the laboratory results [A. Kouchi and T. Kuroda, *Nature* **344**, 134 (1990)] suggests that the time scale for amorphization at Charon's distance from the sun could be as short as 1 hour; however, the weak ultraviolet flux of the sun compared with the laboratory lamp used could make the time scale orders of magnitude longer.
9. W. M. Grundy, M. W. Buie, J. A. Stansberry, J. R. Spencer, B. Schmitt, *Icarus*, in press.
10. We modeled the geometric albedo of an object consisting of spatially distinct regions of pure water ice and a dark neutral material using the absorption coefficients of crystalline water at a temperature of 50 K as measured by W. M. Grundy and B. Schmitt [*J. Geophys Res.* **103**, 25809 (1998)] and the reflectance spectroscopic theory of B. Hapke [*J. Geophys. Res.* **86**, 3039 (1981)]. We assumed grain sizes of 20 μm, which gave the best fit to the depths of the different ice bands.
11. T. B. McCord *et al.*, *J. Geophys. Res.* **104**, 11827 (1999); F. P. Fanale *et al.*, *Icarus* **139**, 179 (1999).
12. The geometric albedo models were constructed by using spatially segregated mixtures combining crystalline water ice, a dark neutral material, and one of the compounds with a 2.2-μm absorption (HCN, NH_3, $NH_3{\cdot}2H_2O$, or alumino silicate clays). A grid search was performed checking all possible ratios of surface coverage of the various components and grain sizes from 2 μm up to 1 mm. Larger grain sizes were not considered because they cause band depths to be too large. For some of the ices, optical constants are not available, so we resorted to scaling the pure reflectance spectra instead of calculating the geometric albedo. Our preferred model uses 20-μm water ice grains at a temperature of 50 K mixed with a dark neutral absorber with an albedo of 4% and ammonia and ammonia hydrate.
13. L. J. Lanzerotti, W. L. Brown, K. J. Marcantonio, R. E. Johnson, *Nature* **312**, 139 (1984).
14. B. Schmitt, E. Quirico, F. Trotta, W. M. Grundy, in *Solar System Ices*, B. Schmitt, C. de Bergh, M. Festou, Eds. (Kluwer Academic, Boston, MA, 1998), pp. 199–241.
15. B. N. Khare *et al.*, *Icarus* **79**, 350 (1989); B. N. Khare *et al.*, *Icarus* **103**, 290 (1993).
16. J. W. Chamberlain and D. M. Hunten, *Theory of Planetary Atmospheres* (Academic Press, Orlando, FL, 1987).
17. J. S. Lewis, *Icarus* **15**, 174 (1971).
18. D. J. Stevenson, *Nature* **298**, 142 (1982); P. M. Schenk, *J. Geophys. Res.* **96**, 1887 (1991); J. S. Kargel, S. K. Croft, J. I. Lunine, J. S. Lewis, *Icarus* **89**, 93 (1992); W. B. Durham, S. H. Kirby, L. A. Stern, *J. Geophys. Res.* **98**, 17667 (1993).
19. S. K. Croft and L. A. Soderblom, in *Uranus*, J. T. Bergstralh, E. D. Miner, M. S. Matthews, Eds. (Univ. of Arizona Press, Tucson, AZ, 1997), pp. 561–628.
20. The spectra of montmorillonite and kaolinite are courtesy of Roger Clark, that of NH_3 is from (*7*), that of $NH_3{\cdot}2H_2O$ is from R. H. Brown, D. P. Cruikshank, A. T. Tokumaga, R. G. Smith, and R. N. Clark [*Icarus* **74**, 262 (1988)], and that of HCN is from D. P. Cruikshank *et al.* [*Icarus* **94**, 345 (1991)].
21. The time rate of sublimation is calculated by assuming equilibrium between the temperature-dependent vapor pressure of the ice [D. R. Lide, Ed., *CRC Handbook of Chemistry and Physics* (CRC Press, Boca Raton, FL, ed. 77, 1996)] and the pressure of the escaping gas immediately above the surface of the object. The temperature is calculated by assuming radiative equilibrium between a pure blackbody and the incoming sunlight.
22. We thank R. Clark and D. Cruikshank for making their spectral data available to us and E. Young and D. Cruikshank for insightful comments on the manuscript. M.E.B. is an Alfred P. Sloan Research Fellow. These data were obtained at the W. M. Keck Observatory, which is operated as a scientific partnership among the California Institute of Technology, the Universities of California, and NASA. The observatory was made possible by the financial support of the W. M. Keck Foundation.

23 September 1999; accepted 6 December 1999

Evidence for a Low-Density Universe from the Relative Velocities of Galaxies

R. Juszkiewicz,[1]* P. G. Ferreira,[1,2,3]† H. A. Feldman,[4] A. H. Jaffe,[5] M. Davis[5]

The motions of galaxies can be used to constrain the cosmological density parameter Ω and the clustering amplitude of matter on large scales. The mean relative velocity of galaxy pairs, estimated from the Mark III survey, indicates that $\Omega = 0.35^{+0.35}_{-0.25}$. If the clustering of galaxies is unbiased on large scales, $\Omega = 0.35 \pm 0.15$, so that an unbiased Einstein–de Sitter model ($\Omega = 1$) is inconsistent with the data.

The mean relative velocity for a pair of galaxies at positions $\vec{r}_1$ and $\vec{r}_2$ is $\vec{u}_{12} = H\vec{r}$, where $\vec{r} = \vec{r}_1 - \vec{r}_2$ and the constant of proportionality $H = 100h$ km s^{-1} Mpc^{-1} is the Hubble parameter (*1, 2*). The quantity $0.6 < h < 1$ parameterizes uncertainties in H measurements. This law is an idealization, followed by real galaxies only on sufficiently large scales, corresponding to a uniform mass distribution. On smaller scales, the gravitational field induced by galaxy clusters and voids generates local deviations from the Hubble flow, called peculiar velocities. Correcting for this effect gives $\vec{u}_{12} = H\vec{r} + v_{12}\vec{r}/r$. The quantity $v_{12}(r)$ is called the mean pairwise streaming velocity. In the limit of large r, $v_{12} = 0$. In the opposite limit of small separations, $u_{12}(r) = 0$ (virial equilibrium). Hence, at intermediate separations, $v_{12} < 0$ and we can expect to observe gravitational infall, or the "mean tendency of well-separated galaxies to approach each other" (*3*). In a recent paper, we derived an expression, relating v_{12} to cosmological parameters (*4*); in another, using Monte Carlo simulations, we showed how v_{12} can be measured from velocity-distance surveys of galaxies (*5*). Our purpose here is to estimate $v_{12}(r)$ from observations and constrain the cosmological density parameter Ω.

The statistic we consider was introduced in the context of the Bogoliubov-Born-Green-Kirkwood-Yvon (BBGKY) kinetic theory describing the dynamical evolution of a self-gravitating collection of particles (*3, 6*). One of the BBGKY equations is the pair conservation equation, relating the time evolution of v_{12} to $\xi(r)$, the two-point correlation function of spatial fluctuations in the fractional matter density contrast (*3*). Its solution is well approximated by (*4*)

$$v_{12}(r) = -\frac{2}{3} Hr\Omega^{0.6}\bar{\bar{\xi}}(r)[1 + \alpha\bar{\bar{\xi}}(r)] \tag{1}$$

$$\bar{\bar{\xi}}(r) = \frac{3\int_0^r \xi(x)x^2dx}{r^3[1 + \xi(r)]} \tag{2}$$

where $\alpha = 1.2 - 0.65\gamma$, $\gamma = -(d \ln \xi/d \ln$

[1]Département de Physique Théorique, Université de Genève, CH-1211 Genève, Switzerland. [2]Theory Group, CERN, CH-1211 Genève 23, Switzerland. [3]CENTRA, Instituto Superior Tecnico, Lisboa 1096 Codex, Portugal. [4]Department of Physics and Astronomy, University of Kansas, Lawrence, KS 66045, USA. [5]Center for Particle Astrophysics, University of California, Berkeley, CA 94720, USA.

*On leave from Copernicus Astronomical Center, 00-716 Warsaw, Poland.
†To whom correspondence should be addressed. E-mail: pgf@astro.ox.ac.uk

$r)_{\xi=1}$, and Ω is the present density of nonrelativistic particles. Equations 1 and 2 were obtained by interpolating between a second-order perturbative solution for $v_{12}(r)$ and the nonlinear stable clustering solution. For a particle pair at separation $\vec{r}$, the streaming velocity is given by

$$v_{12}(r) = \langle(\vec{v}_1 - \vec{v}_2)\cdot\hat{r}\rangle_\rho = \langle(\vec{v}_1 - \vec{v}_2)\cdot\hat{r}w_{12}\rangle \quad (3)$$

where $w_{12} = (1 + \delta_1)(1 + \delta_2)[1 + \xi(r)]^{-1}$ is the pair-density weighting; $\vec{v}_A$ and δ_A are the peculiar velocity and fractional density contrast of matter at position $\vec{r}_A$, respectively; $A = 1, 2\cdots$; the separation $r = |\vec{r}_1 - \vec{r}_2|$ is fixed for all pairs; the circumflexes denote unit vectors; and $\xi(r) = \langle\delta_1\delta_2\rangle$. The expression in square brackets in the definition of w_{12} ensures that $\langle w_{12}\rangle = 1$ and the pairwise velocity probability density integrates to unity. The pair-weighted average, $\langle\cdots\rangle_\rho$, differs from simple spatial averaging, $\langle\cdots\rangle$, by the weighting factor w_{12}. The pair-weighting makes the average different from zero, unlike the volume average, $\langle\vec{v}_1 - \vec{v}_2\rangle \equiv 0$, which vanishes because of isotropy.

Our approximate solution of the pair conservation equation was successfully tested against N-body simulations in the dynamical range $\xi \le 10^3$ (*4, 7*). It is valid for universes filled with nonrelativistic particles, and it is insensitive to the value of the cosmological constant (*2, 4*). Equation 1 was derived under the additional assumption that the probability distribution of the initial, small-amplitude density fluctuations was Gaussian.

Until now, we have also implicitly assumed (i) that the spatial distribution of galaxies traces the mass distribution and (ii) that $v_{12}(r)$ for the galaxies is the same as that for the matter. If the galaxies are more clustered than mass, condition (i) is broken and we have "clustering bias." The galaxy two-point correlation function is close to a power law, $\xi^{\rm gal}(r) \propto r^{-\gamma}$, over three orders of magnitude in separation r (*8*). This is not true for the mass correlation function $\xi(r)$ in structure formation models of the cold dark matter (CDM) family (*7*). To reconcile theory with observation, one has to introduce a measure of bias that depends on separation and cosmological time t: $b^2(r,t) = \xi^{\rm gal}(r,t)/\xi(r,t)$. Because of the pair-density weighting, clustering bias can in principle induce "velocity bias" in a way similar to systematic error propagation. This is certainly true in the most simplistic of all biasing prescriptions, the "linear biasing," under which b is a constant and, moreover, $\delta^{\rm gal} = b\delta$. The expression for $v_{12}^{\rm gal}$ can be obtained from Eq. 3 by formally replacing the weighting function $w_{12}(\delta_1,\delta_2)$ with $w_{12}(\delta_1^{\rm gal}, \delta_2^{\rm gal})$. In the linear limit $\xi \ll 1$, we get $v_{12}^{\rm gal} = bv_{12}$ (*9*), in qualitative agreement with recent N-body simulations, which considered a whole range of biasing prescriptions, allowing nonlinear or nonlocal mapping (or both) of the mass density field onto $\delta^{\rm gal}$ (*10*). However, there are also simulations that show exactly the opposite: Although the galaxies do not trace the spatial distribution of mass, pairs of galaxies behave like pairs of test particles moving in the gravitational field of the true mass distribution, and $v_{12}^{\rm gal}(r) = v_{12}(r)$ (*11*). Direct measurements of $v_{12}^{\rm gal}(r)$ can help us decide which simulations and biasing schemes are more believable than others. Indeed, one can measure $v_{12}^{\rm gal}$ for different morphological classes of galaxies. The linear bias model predicts $v_{12}^{\rm (E)}/v_{12}^{\rm (S)} = b^{\rm (E)}/b^{\rm (S)}$, where the superscripts refer to elliptical (E) and spiral (S) galaxies. Observations suggest $b^{\rm (E)}/b^{\rm (S)} \approx 2$ and $b^{\rm (S)} \approx 1$ (*12*). Hence, one expects $v_{12}^{\rm (E)}/v_{12}^{\rm (S)} \approx 2$ if the linear bias model is correct and $v_{12}^{\rm (E)}/v_{12}^{\rm (S)} = 1$ in the absence of velocity bias.

Measurements of $v_{12}(r)$ can be also used to determine Ω. Indeed, if the mass correlation function is well approximated by a power law, $\xi(r) \propto r^{-\gamma}$, v_{12} at a fixed separation can be expressed in terms of Ω and the standard normalization parameter σ_8. The latter quantity is the root-mean-square contrast in the mass found within a randomly placed sphere of radius $8h^{-1}$ Mpc. Unlike the conventional linear perturbative expression for $v_{12}(r) \propto \Omega^{0.6}\sigma_8^2 r^{1-\gamma}$, our nonlinear ansatz provides the possibility of separating σ_8 from Ω by measuring v_{12} at different values of r [see the bottom panel in Fig. 1; also see (*13*)].

We will now describe our measurements. The mean difference between radial velocities of a pair of galaxies is $\langle s_A - s_B\rangle_\rho = v_{12}\,\hat{r}\cdot(\hat{r}_A + \hat{r}_B)/2$, where $s_A = \hat{r}_A\cdot\vec{v}_A$ and $\vec{r} = \vec{r}_A - \vec{r}_B$. Here as before, the subscript letters number the galaxies in the survey ($A, B = 1, 2\cdots$). To estimate v_{12}, we minimize the quantity $\chi^2(v_{12}) = \Sigma_{A,B}\,[(s_A - s_B) - p_{AB}v_{12}/2]^2$, where $p_{AB} \equiv \hat{r}\cdot(\hat{r}_A + \hat{r}_B)$ and the sum is over all pairs at fixed separation $r = |\vec{r}_A - \vec{r}_B|$. The resulting statistic is (*5*)

$$v_{12}(r) = \frac{2\sum(s_A - s_B)p_{AB}}{\sum {p_{AB}}^2} \quad (4)$$

Monte Carlo simulations show that this estimator is insensitive to biases in the way that galaxies are selected from the sky and can be corrected for biases due to errors in the estimates of the radial distances to the galaxies (*5*). The survey used here is the Mark III standardized catalog of galaxy peculiar velocities (*14–16*). It contains 2437 spiral galaxies with Tully-Fisher (TF) distance estimates and 544 ellipticals with $D_n - \sigma$ distances. The total survey depth is over $120h^{-1}$ Mpc, with homogenous sky coverage up to $30h^{-1}$ Mpc. The inverse TF and Infrared Astronomical Satellite (IRAS) density field corrections for inhomogeneous Malmquist bias in the spiral sample agree with each other and give similar streaming velocities, with lognormal distance errors of order $\sigma_{\ln d} \approx 23\%$. For the elliptical sample, $\sigma_{\ln d} \approx 21\%$, and the distances assume a smooth Malmquist bias correction (*17*).

The estimates from the spiral and elliptical galaxies are remarkably consistent with each other (Fig. 1), unlike previous comparisons using the velocity correlation tensor (*18, 19*). For a velocity ratio $R = v_{12}^{\rm (E)}/v_{12}^{\rm (S)} = 1$, we obtain $\chi^2 \simeq 1$, whereas for $R = 2$, $\chi^2 = 2.1$. The most straightforward interpretation of this result is that there is no velocity bias and the linear clustering bias model should be rejected. Its static character and the resulting failure to describe particle motion, induced by gravitational instability, was pointed out earlier on theoretical grounds (*20*). Our results can, however, be reconciled with a linear bias model if it is generalized to allow scale dependence, $b = b(r)$. Biasing factors for both galaxy types can be arbitrarily large at small separations, where $\xi(r) \gg 1$, if biasing is suppressed at large separations, where $|\xi(r)| < 1$. Indeed, in the nonlinear limit, $w_{12}(b\delta_1, b\delta_2) \to b^2\delta_1\delta_2/b^2\xi = \delta_1\delta_2/\xi$, and hence, $v_{12}^{\rm gal}(r) \to v_{12}(r)$.

We obtained an estimate of σ_8 and Ω from the shape of the $v_{12}(r)$ profile as follows. We

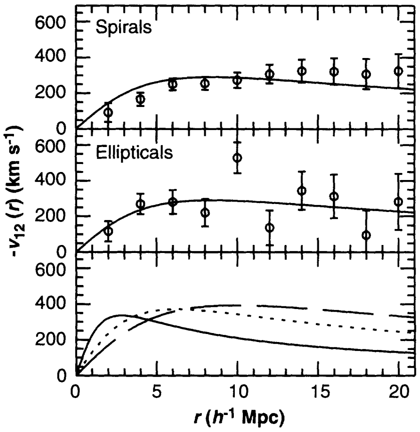

Fig. 1. The streaming velocities of 2437 spiral galaxies (top) and 544 elliptical galaxies (middle) estimated from the Mark III catalog. The error bars are the estimated 1σ uncertainties in the measurement due to lognormal distance errors, sparse sampling (shot noise), and finite volume of the sample (sample variance). The error bars were estimated from mock catalogs described in (*5*). The small sample volume also introduces correlations between measurements of $v_{12}(r)$ at different values of r. To guide the eye and to show that, although the two samples have different noise levels (because of much smaller number of galaxies in the elliptical sample), the $v_{12}(r)$ signal in both cases is similar, we also plot $v_{12}(r)$ calculated from Eq. 1 for a $\xi \propto r^{-1.75}$ power-law model with $\sigma_8 = 1.25$ and $\Omega = 0.3$. Three theoretical $v_{12}(r)$ curves are plotted (bottom) with $\xi \propto r^{-1.75}$, $\sigma_8\Omega^{0.6} = 0.7$, and $\sigma_8 = 0.5$ (solid curve), 1 (dotted curve), and 1.5 (dashed curve). These curves show how measurements of $v_{12}(r)$ can break the degeneracy between Ω and σ_8.

assumed that the shape of the mass correlation function $\xi(r)$ (but not necessarily the amplitude) is similar to the shape of the galaxy correlation function estimated from the automatic plate measuring system (APM) catalog (*8*), consistent with a power-law index $\gamma = 1.75 \pm 0.1$ (the errors we quote are conservative) for separations $r \leq 10h^{-1}$ Mpc. Given the depth of the Mark III catalog, we expect the covariance between estimates of $v_{12}(r)$ to be only weakly correlated at $r < 10h^{-1}$ Mpc; we use *N*-body simulations to determine the covariance of the estimates over this range of scales and use a χ^2 minimization to obtain the 1σ constraints: $\sigma_8 \geq 0.7$ and $\Omega = 0.35^{+0.35}_{-0.25}$. Fixing $\sigma_8 = 1$, we obtain $\Omega = 0.35 \pm 0.15$ (Fig. 2).

We can obtain a more conservative constraint on σ_8 and Ω by examining a v_{12} at a single separation, $r \equiv r_* = 10h^{-1}$ Mpc. Substituting $r = r_*$ and $\xi(r) \propto r^{-1.75}$ into Eqs. 1 and 2, we get

$$v_{12}(r_*) = -605\sigma_8{}^2\Omega^{0.6}(1 + 0.43\sigma_8{}^2)/(1 + 0.38\sigma_8{}^2)^2 \text{ km s}^{-1} \quad (5)$$

The above relation shows that, at $r = r_*$, v_{12} is almost entirely determined by the values of two parameters: σ_8 and Ω. The uncertainties in the observed γ lead to an error in Eq. 5 of <10% for $\sigma_8 \leq 1$. In fact, at this level of accuracy and at this particular scale, our constraints depend only on the value of Ω and the overall normalization σ_8 but do not depend on other model parameters, such as the shape of $\xi(r)$. The streaming velocity $v_{12}(r_*)$ depends on $\xi(r)$ only at $r < r_*$, so unlike bulk flows, it is unaffected by the behavior of $\xi(r)$ at $r > r_*$ [compare our Eq. 1 with equation 21.76 in (*2*)]. Moreover, the dominant contribution to $v_{12}(r_*)$ comes from $\bar{\xi}(r_*)$, an average of $\xi(r)$ over a ball of radius r_*, so the details of the true shape of $\xi(r)$ at $r < r_*$ have little effect on $v_{12}(r_*)$ as long as σ_8 (and hence, the volume-averaged ξ) is fixed. Thus, Eq. 5 can provide robust limits on σ_8 and Ω, even if the assumption about the proportionality of $\xi(r)$ to the APM correlation function is dropped. This statement can be directly tested by comparing predictions of Eq. 5 with predictions of CDM-like models, all of which fail to reproduce the pure power-law behavior of the observed galaxy correlation function. When this test was applied to four models, recently simulated by the Virgo Consortium (*7*), we found that, for fixed values of σ_8 and Ω, the predictions based on Eq. 5 were within ≤6% of $v_{12}(r_*)$, obtained from the simulations (*21*). The measured value, $-v_{12}(r_*) = 280^{+68}_{-53}$ km s^{-1} (Fig. 1), is inconsistent with $\sigma_8 = 1$ and $\Omega = 1$ at the 99% confidence level.

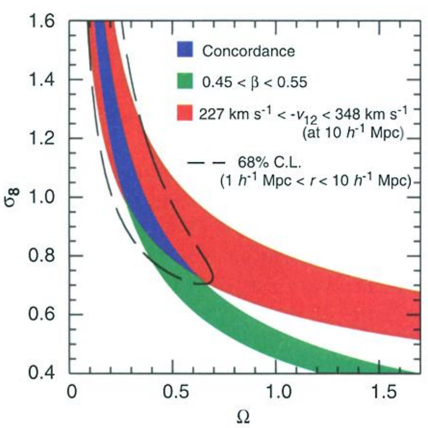

Fig. 2. The blue region constrains the viable values of Ω, the fractional mass density of the universe, and σ_8 (the variance of mass fluctuations at $r = 8h^{-1}$ Mpc) from the combination of the constraints on the streaming velocities (red region) and $\beta = \sigma_8\Omega^{0.6}$ (green region). The streaming velocities are constrained at $r = 10h^{-1}$ Mpc from the Mark III catalog of peculiar velocities, and β is measured with the VELMOD comparison between the Mark III catalog and the velocity field inferred from the IRAS redshift survey. The dashed curve defines the 1σ obtained from comparing expressions 1 and 2 with the Mark III catalog from $2h^{-1}$ to $10h^{-1}$ Mpc (C.L., confidence level).

Our results are compatible with a number of earlier dynamical estimates of the parameter $\beta \equiv \Omega^{0.6}\sigma_8$ [β is sometimes defined as $\Omega^{0.6}/b$, but $\sigma_8 \approx 1/b$ and the two definitions differ at the 10% level at most; see, for example, (*8*)]. A technique, based on the action principle (*22*), gives $\beta = 0.34 \pm 0.13$; comparisons of peculiar velocity fields with redshift surveys based on the integral form of the continuity equation (called velocity-velocity comparisons) typically give $\beta = 0.5 - 0.6$ (*23–26*). Of the velocity-velocity comparisons, the one with the smallest error bars is the VELMOD estimate: $\beta = 0.5 \pm 0.05$ (*24*). This constraint has several advantages over others; in particular, it correctly takes into account cross-calibration errors between different Mark III subcatalogs. To illustrate the consistency of our results with velocity-velocity studies, we will now compare our limits on σ_8 and Ω, derived from the shape of $v_{12}(r)$ for a range of separations with constraints from our measurement of $v_{12}(10h^{-1}$ Mpc) alone, combined with limits from VELMOD (Fig. 2). Again, we find that a low-Ω universe is favored: $\Omega < 0.65$ and $\sigma_8 > 0.7$. The concordance region overlaps with the constraint derived from our measurements of $v_{12}(r)$.

Our results disagree with the IRAS-POTENT estimate, $\beta = 0.89 \pm 0.12$ (*27*). The IRAS-POTENT analysis is based on the continuity equation in its differential form; it uses a rather complicated reconstruction technique to recover the full velocity field from its radial component. The reason for the disagreement is not clear at present. We can think of at least two possible sources of systematic errors in the IRAS-POTENT analysis: (i) the reconstruction scheme itself (for example, taking spatial derivatives of noisy data) and (ii) the nonlinear corrections adopted. The nonlinear corrections diverge like $\Omega^{-1.8}$ in the limit $\Omega \rightarrow 0$ (*27*). By contrast, the accuracy of the nonlinear corrections for the velocity-velocity approach is insensitive to Ω. The velocity-velocity approach is also simpler than IRAS-POTENT because it does not involve the reconstruction of the full velocity vector from its radial component measurements (although both approaches require a reconstruction of galaxy positions from their redshifts). Our method is direct, not inverse: It does not require any reconstruction at all.

Finally, there is a potential caveat in the "no velocity bias" assumption in our own analysis. Although this assumption is based on empirical evidence from the two sets of galaxy types, the observational data are noisy and involve nontrivial corrections for Malmquist bias, which could affect the two samples differently. Application of our approach to different data sets should clarify these issues. If, contrary to our preliminary results, the streaming velocity turns out to be subjected to bias after all, such a finding may affect our estimates of σ_8 and Ω, based on the shape of the $v_{12}(r)$ profile but not on our rejection of the unbiased Einstein–de Sitter model. In this sense, our differences with the IRAS-POTENT analysis do not depend on the presence or absence of velocity bias.

The advantages of the statistic we have used here can be summarized as follows. First, v_{12} can be estimated directly from velocity-distance surveys, without subjecting the observational data to multiple operations of spatial smoothing, integration, and differentiation, which are used in various reconstruction schemes. Second, unlike cosmological parameter estimators based on the acoustic peaks, expected to appear in the cosmic microwave background power spectrum (*28*), the Ω estimate based on v_{12} is model independent. Finally, our approach offers the possibility of breaking the degeneracy between Ω and σ_8 by measuring $v_{12}(r)$ at different separations.

References and Notes

1. E. P. Hubble, *Proc. Natl. Acad. Sci. U.S.A.* **15**, 168 (1929).
2. P. J. E. Peebles, *Principles of Physical Cosmology* (Princeton Univ. Press, Princeton, NJ, 1993), pp. 340–342.
3. ———, *The Large-Scale Structure of the Universe* (Princeton Univ. Press, Princeton, NJ, 1980), pp. 266–268.
4. R. Juszkiewicz, V. Springel, R. Durrer, *Astrophys. J.* **518**, L25 (1999).
5. P. G. Ferreira, R. Juszkiewicz, H. Feldman, M. Davis, A. H. Jaffe, *Astrophys. J.* **515**, L1 (1999).
6. M. Davis and P. J. E. Peebles, *Astrophys. J. Suppl. Ser.* **34**, 425 (1977).
7. A. Jenkins *et al.*, *Astrophys. J.* **499**, 20 (1998).

8. G. Efstathiou, in *Les Houches, Session LX: Cosmology and Large Scale Structure*, R. Schaeffer *et al.*, Eds. (North-Holland, Amsterdam, 1996), pp. 107–252.
9. K. B. Fisher, M. Davis, M. Strauss, A. Yahil, J. Huchra, *Mon. Not. R. Astron. Soc.* **267**, 927 (1994).
10. V. K. Narayanan, A. Berlind, D. H. Weinberg, available at http://xxx.lanl.gov/abs/astro-ph/9812002.
11. G. Kauffmann, J. M. Colberg, A. Diaferio, S. D. M. White, *Mon. Not. R. Astron. Soc.* **303**, 188 (1999). To linear bias enthusiasts, this result may appear puzzling. A textbook example of such a possibility is the spatial distribution of the gas and stars in a galaxy. Their distribution itself is biased, whereas their relative velocities at separations comparable to the radius of the dark halo are not.
12. M. A. Strauss and J. A. Willick, *Phys. Rep.* **261**, 271 (1995).
13. *N*-body simulations show that the stable clustering solution $[u_{12} = 0, -v_{12}(r)/Hr = 1]$ occurs for $\xi > 200$ [(*7*); see also B. Jain, *Mon. Not. R. Astron. Soc.* **287**, 687 (1997)]. In the limit $r \rightarrow 0$, our ansatz gives $-v_{12}/Hr \rightarrow [2/(3-\gamma)]\Omega^{0.6}(1+\alpha)$, which for the range of parameters considered is generally different from unity (although of the right order of magnitude). It is possible to improve our approximation and satisfy the small separation boundary condition by replacing $(2/3)\Omega^{0.6}$ with the expression $[(1-\gamma/3)F\xi(r) + (2/3)\Omega^{0.6}]/[F\xi(r)+1]$, where $F \approx 1/100$ is a fudge factor ensuring that $-v_{12}/Hr \rightarrow 1$ when $\xi \gg 100$, while the perturbative, large-scale solution remains unaffected. However, the stable clustering occurs at separations smaller than $200h^{-1}$ kpc, which is a tenth of the smallest separation we consider here. As a result, in our range of separations *r*, Eq. 1 is as close to fully nonlinear *N*-body simulations as the improvement, suggested above [see (*4*) and Fig. 2].
14. J. A. Willick, S. Courteau, S. M. Faber, D. Burstein, A. Dekel, *Astrophys. J.* **446**, 12 (1995).
15. J. A. Willick, *et al.*, *Astrophys. J.* **457**, 460 (1996).
16. J. A. Willick *et al.*, *Astrophys. J. Suppl. Ser.* **109**, 333 (1997).
17. D. Lynden-Bell *et al.*, *Astrophys. J.* **329**, 19 (1988).
18. K. M. Górski, M. Davis, M. A. Strauss, S. D. M. White, A. Yahil, *Astrophys. J.* **344**, 1 (1989).
19. E. J. Groth, R. Juszkiewicz, J. P. Ostriker, *Astrophys. J.* **346**, 558 (1989).
20. Under realistic circumstances, one expects that gravitational growth of clustering pulls the mass with the galaxies. As a result, any clustering bias, introduced at the epoch of galaxy formation, is likely to evolve toward unity at late times, at variance with the linear bias model, where *b* is time independent [J. N. Fry, *Astrophys. J.* **461**, L65 (1996); P. J. E. Peebles, available at http://xxx.lanl.gov/abs/astro-ph/9910234]. A similar behavior was seen in *N*-body simulations (*11*). The linear bias relation $\delta^{gal} = b\delta$ is a conjecture that generally does not follow from the relation between the correlation functions $\xi^{gal} = b^2\xi$ unless we restrict our model to a narrow subclass of random fields.
21. Imagine that one of the CDM-like models is a valid description of our universe. Let us choose the dark energy and CDM (ΛCDM) model, recently simulated by the Virgo Consortium (*7*). It is defined by parameters $h = 0.7$, $\Omega = 0.3$, $\sigma_8 = 0.9$, and $\Omega_\Lambda = 0.7$, which is the cosmological constant's contribution to the density parameter. This model requires scale-dependent biasing because the predicted shape of $\xi(r)$ differs widely from the observed galaxy correlation function: At separations hr Mpc^{-1} = 10, 4, 2, and 0.1, the logarithmic slope of the mass correlation function reaches the values, given by $\gamma = 1.7$, 1.5, 2.5, and 1, respectively. As we expected, however, these wild oscillations do not affect the resulting $v_{12}(r_*)$. Indeed, the *N*-body simulations (*7*) give $v_{12}(r_*) = -220$ km s^{-1}, and substituting $\sigma_8 = 0.9$ and $\Omega = 0.3$ in Eq. 5 gives $v_{12}(r_*) = -225$ km s^{-1}.
22. E. J. Shaya, P. J. E. Peebles, R. B. Tully, *Astrophys. J.* **454**, 15 (1995).
23. M. Davis, A. Nusser, J. A. Willick, *Astrophys. J.* **473**, 22 (1996).
24. J. A. Willick, M. A. Strauss, A. Dekel, T. Kolatt, *Astrophys. J.* **486**, 629 (1997).
25. L. N. da Costa *et al.*, *Mon. Not. R. Astron. Soc.* **299**, 425 (1998).
26. J. A. Willick and M. A. Strauss, *Astrophys. J.* **507**, 64 (1998).
27. Y. Sigad, A. Eldar, A. Dekel, M. A. Strauss, A. Yahil, *Astrophys. J. Suppl. Ser.* **109**, 516 (1997).
28. A. G. Doroshkevich, Ya. B. Zeldovich, R. A. Sunyaev, *Sov. Astron.* **22**, 523 (1978).
29. We are grateful to L. da Costa for encouragement at the early stages of this project. We also benefited from discussions with S. Courteau, R. Durrer, K. Górski, and J. Peebles. R.J. was supported by the State Committee for Scientific Research (KBN) (Poland), the Tomalla Foundation (Switzerland), and the Poland-U.S. M. Skłodowska-Curie Fund. M.D. and A.H.J. were supported by grants from NSF and NASA. H.A.F. and R.J. were supported by NSF-EPSCOR and the General Research Fund. We thank the organizers of the summer 1997 workshop at the Aspen Center for Physics, where this work began.

12 August 1999; accepted 10 November 1999

The Changing Morphology and Increasing Deceleration of Supernova 1993J in M81

N. Bartel,[1]* M. F. Bietenholz,[1] M. P. Rupen,[2] A. J. Beasley,[2] D. A. Graham,[3] V. I. Altunin,[4] T. Venturi,[5] G. Umana,[6] W. H. Cannon,[1,7] J. E. Conway[8]

Twenty consecutive Very Long Baseline Interferometry images of supernova 1993J from the time of explosion to the present show the dynamic evolution of the expanding radio shell of an exploded star. High-precision astrometry reveals that the supernova expands isotropically from its explosion center. Systematic changes in the images may reflect a pattern of anisotropies and inhomogeneities in the material left over from the progenitor star. As the shock front sweeps up the material in the surrounding medium, it is increasingly decelerated and influenced by the material. After 5 years, the supernova has slowed to half of its original expansion velocity and may have entered the early stages of the adiabatic phase common in much older supernova remnants in the Milky Way Galaxy.

Supernova 1993J (SN1993J) (*1*) in the nearby galaxy M81 was the brightest optical supernova in the Northern Hemisphere since SN1954A and, at a distance of only 3.63 ± 0.36 Mpc (*2*), among the closest in modern history. Its progenitor star is believed to have been either an ~15-solar-mass ($M_\odot$) supergiant that has lost a substantial portion of its hydrogen envelope to a companion in a binary system (*3, 4*) or a single ~30$M_\odot$ supergiant (*5*). Shock breakout from the explosion occurred on 28.0 March 1993 UT (*6*). Radio emission was detected a few days thereafter (*7*). An optical image of M81 superimposed on a 5-GHz Very Large Array (VLA) radio map shows the supernova in a southern spiral arm (Fig. 1). Very Long Baseline Interferometry (VLBI) observations of the young radio source during the first 100 days showed that its size was growing with time *t*, with the angular radius $\theta \propto t^m$ and $m = 0.96 \pm 0.07$ (*8*). As the supernova expanded, its shell-like structure was revealed (*9, 10*). The expansion was found to be decelerated over a time of ~3 years, with estimates of *m* of 0.86 ± 0.02 (*11*) and 0.837 ± 0.025 (*12*). The nature of the expansion was reported (*11*) to be self-similar, as described in the standard model (*13*) of the interaction of the shock front with the circumstellar medium (CSM) left over from the mass loss of the progenitor star. The structure of the supernova would remain unchanged in this model except for a time-dependent scaling factor, and the deceleration would be constant. Here, we present results from VLBI observations over 5 years (*14*) and show that the structure of SN1993J is changing while the expansion remains isotropic but increasingly decelerates, together reflecting departures from a self-similar evolution and revealing insights into how several-hundred–year-old supernova remnants in the Milky Way Galaxy may have evolved.

Twenty consecutive images of SN1993J were acquired from about 50 days to 5 years after the shock breakout (Fig. 2). They were made from VLBI data at 8.4 GHz phase-referenced to the core (*15*) of M81. The earliest image of SN1993J shows an almost

[1]Department of Physics and Astronomy, York University, Toronto M3J 1P3, Ontario, Canada. [2]National Radio Astronomy Observatory, Socorro, NM 87801, USA. [3]Max-Planck-Institut für Radioastronomie, D-53121 Bonn, Germany. [4]Jet Propulsion Laboratory, California Institute of Technology, Pasadena, CA 91109, USA. [5]Instituto di Radioastronomia, CNR, 40129 Bologna, Italy. [6]Instituto di Radioastronomia, CNR, 96017 Noto, Italy. [7]Space Geodynamics Laboratory/CRESTech, Toronto M3J 3K1, Ontario, Canada. [8]Onsala Space Observatory, Chalmers University of Technology, S-43992 Onsala, Sweden.

*To whom correspondence should be addressed. E-mail: bartel@york.u.ca